Measurements and Predictive Models for the *N*-Methyl-2-pyrrolidone/Water/Methanol System

Santiago Aparicio,* Rafael Alcalde, María J. Dávila, Begoña García, and José M. Leal*

Departamento de Química, Universidad de Burgos 09001 Burgos, Spain

Received: December 28, 2007; Revised Manuscript Received: May 8, 2008

This work reports on the properties and structure of *N*-methyl-2-pyrrolidone in binary and ternary liquid mixtures with water and/or methanol. A comprehensive set of thermophysical properties have been measured at 298.15 K and 0.1 MPa over the whole composition range. On the basis of the derived excess and mixing properties, the fluid structure was analyzed by looking into the forces and geometry factors that effectively control the mixture behavior. Application of the inverted Kirkwood−Buff theory provides a reasonable link between the macroscopic properties and the microscopic features. A density functional theory computation was carried out to analyze the structure and energy features of the hydrogen bonded complexes formed between the components. Use of semiempirical models in the framework of molecular-based equations of state according to the PC-SAFT approach led to unsatisfactory predicted thermophysical properties. The conclusions arrived at give away the existence of strong heteroassociations and hydrogen bonding self-associations that determine the complex nature of the fluid structure.

Introduction

The properties of liquid mixtures bear a practical interest both in technological[1] and theoretical[2] applications. Multicomponent solvents are almost ubiquitous and have found a place in settings such as pharmaceutical, agrochemical and petrochemical industries,[3] often on a multiton scale. Moreover, the growing green sensibility has given way to stricter environment regulations such that, to increase production targets minimizing waste materials, the design of processes requires precise thermophysical properties of the fluids involved.[4] Likewise, achievement of structure−property relationships of multicomponent systems linking the macroscopic properties with microscopic features, intermolecular forces and geometry effects is advisable. However, the performance of accurate measurements over wide pressure and temperature ranges is time-consuming and requires an expensive instrumentation that often is unavailable.[5] A fairly nice route to overcome such a mismatch consists of combining improved molecular based designs with solvents properly selected on the basis of the macroscopic properties and the microscopic features.[6]

N-Methyl-2-pyrrolidone (NMP), the lactam of 4-methylaminobutyric acid (Figure 1), is a weakly basic, thermically and chemically stable volatile organic solvent (VOC)[7] with low vapor pressure (0.373 kPa at 330 K)[8] and reduced teratogenic ability;[9] it is easily biodegradable,[10] nontoxic for aquatic life and can, therefore, replace advantageously other solvents with less favorable toxicological profile or ozone-depleting ability. NMP is strongly polar (μ_{30C} = 4.09 D)[11] with a remarkable dipolar ordering and a noticeable H-bonding acceptor ability through the CO oxygen, and can be useful to recover aromatics, for gas desulfuration,[1] and to produce butadiene, thermo resistant polymers or surface coatings. The NMP environment profile may be improved upon mixing with water (W) and methanol (M), forming complex structures. The selectivity and capability of these solvent blends is affected by the cosolvent amount and can be regulated through the mixture composition.[12,13]

In this work, the NMP + W + M ternary system and the NMP + W, NMP + M and W + M binary constituents were looked into at 298.15 K and 0.1 MPa over the full composition range. The study intends to draw molecular level information from the macroscopic properties; the conclusions raised, confirmed by density functional theory (DFT) calculations in the gas phase and in solution, point to NMP/W and NMP/M complexes. The structural complexity added by the inherent H-bonding effects make the accurate prediction of the properties for the above mixtures challenging. Although a qualitative connection between the macroscopic and microscopic features is feasible, quantitative conclusions are difficult to reach and should be regarded only as simplified. Hence, the inverted Kirkwood−Buff (KB) theory[14] was used to attain reliable molecular-level information from the macroscopic data; this is an exact statistical mechanics model that provides a mathematical link between macroscopic data and preferential solvation. Simple, reliable models capable of predicting mixture properties for process design have been applied on the basis of two different approaches: (i) semiempirical predictive models,[15] and (ii) equations of state (EOS) according to the perturbed chain statistical associating fluid theory PC-SAFT.[16]

To this aim, Scheme 1 displays the organizational array of this work, which covers the following stages: (a) accurate measurement of the thermophysical data needed for industrial applications that best characterize the fluids behavior and serve to validate theoretical models; (b) quantum mechanics calculations that may provide valuable information on the molecular interactions affecting the fluids structure; (c) a KB study that provides reliable molecular level insights from macroscopic properties and enables to settle structure-composition relationships; (d) application of the PC-SAFT model for process design as a useful tool that combines accuracy, computational simplicity and strong molecular foundation; (e) application of semiempirical models useful for engineering purposes and adequate to predict thermophysical properties of complex systems.

* Corresponding authors. E-mail: (S.A.) sapar@ubu.es; (J.M.L.) jmleal@ubu.es.

10.1021/jp712131j CCC: $40.75
Published on Web 08/15/2008

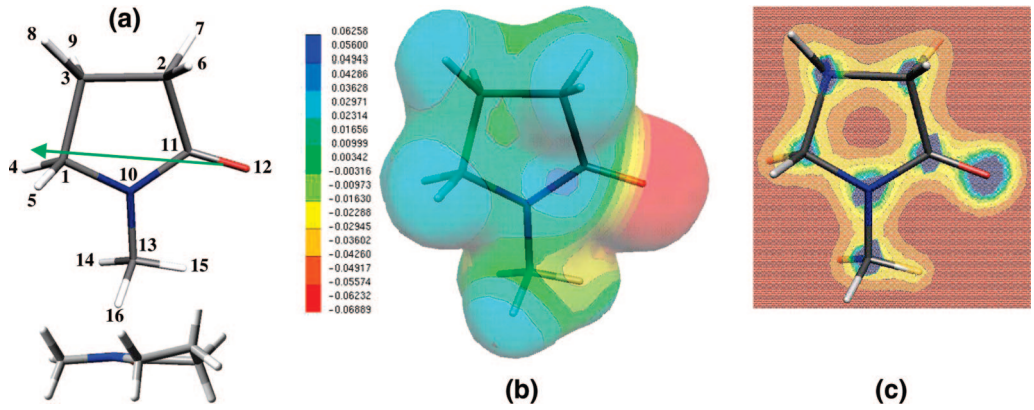

Figure 1. NMP (a) optimized structure and view across the ring, (b) electrostatic potential mapped on an electronic density surface isovalue of 0.0005 au and (c) slice through the electron density isosurface on a plane containing the molecular ring, calculated at B3LYP/6-311++g** theoretical level in gas phase. Atom color code: gray = carbon, white = hydrogen, red = oxygen and blue = nitrogen. In ESP: red = negative, blue = positive. Green arrow shows calculated dipole moment.

SCHEME 1

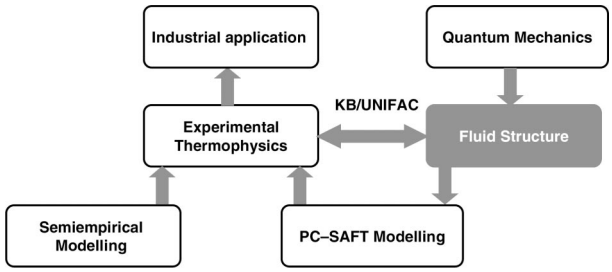

Materials and Methods

Thermophysics. The solvents NMP (Fluka, purity >99.0%) and M (Fluka, purity >99.8%) were used without further purification. Millipore Milli-Q water (resistivity 18.2 mΩ·cm) was used in all experiments. The fluids were degassed with ultrasounds and kept out of the light (NMP is photosensitive) over Fluka 0.3 nm molecular sieves. The purity of NMP and M was checked by GC using a Perkin-Elmer 990 Gas Chromatograph and by comparison with the literature data (Supporting Information Table S1 and refs 17–24). To leave out undesired preferential evaporation, the samples were prepared ($\pm 1 \times 10^{-4}$ mole fraction) by weighing amounts to $\pm 1 \times 10^{-5}$g with a Mettler AT261 balance and syringing them into vials with an equal total volume. Even NMP+W+M sample distributions over the whole composition range were attained as previously described.[25]

Densities (ρ) and speeds of sound (u) were measured simultaneously with an Anton Paar DSA 5000 instrument. Densities were measured ($\pm 5 \times 10^{-6}$ g cm^{-3}) according to the oscillating U-tube principle and speeds of sound (± 0.5 m s^{-1}) by measuring the traveling time through the sample of an impulse from a piezoelectric emission; the cell temperature was controlled by a built-in solid state thermostat and measured by

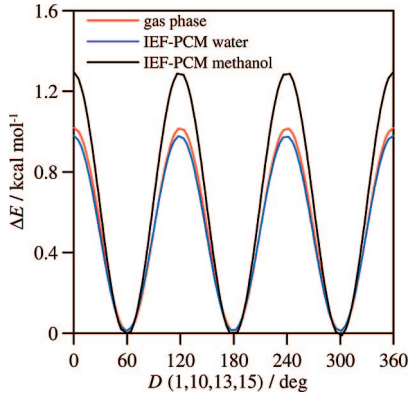

Figure 2. Relaxed potential energy scannings computed at B3LYP/6-311++g** theoretical level for NMP in gas phase, and water and methanol solutions (IEF-PCM). ΔE is the energy relative to the conformer with lower energy. Scanned dihedral angle D(1,10,13,15); atom numbering as in Figure 1.

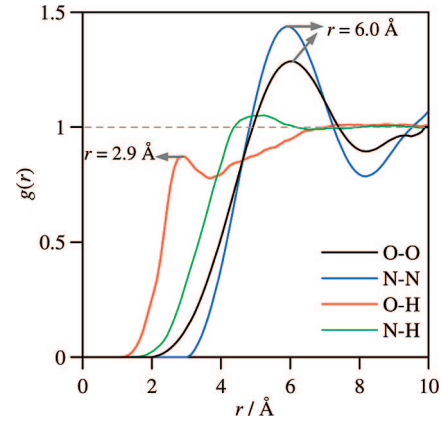

Figure 3. Site−site radial distribution functions, $g(r)$, of pure NMP calculated from NVT molecular dynamics simulations with the OPLS-AA forcefield. O = carbonyl oxygen, N = amino nitrogen, and H = hydrogens in the cycle.

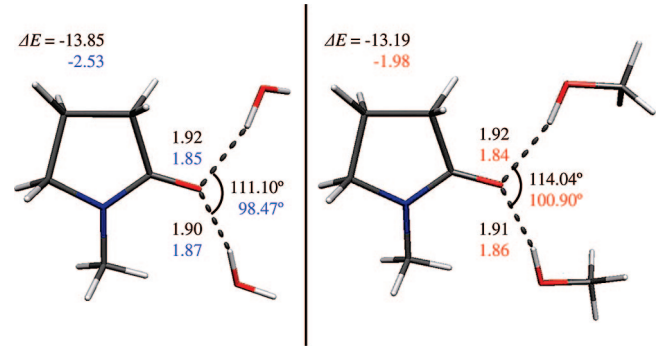

Figure 4. Highest binding energy 1:2 NMP:W (or 1:2 NMP:M) complexes calculated at B3LYP/6-311++g** theoretical level in gas phase and W and M (IEF-PCM) solutions. Atom color code as in Figure 1. Distance in Å, counterpoise corrected binding energies (ΔE) in kcal mol^{-1}. Labels: (black) gas phase, (blue) IEF-PCM water, and (red) IEF-PCM methanol solutions.

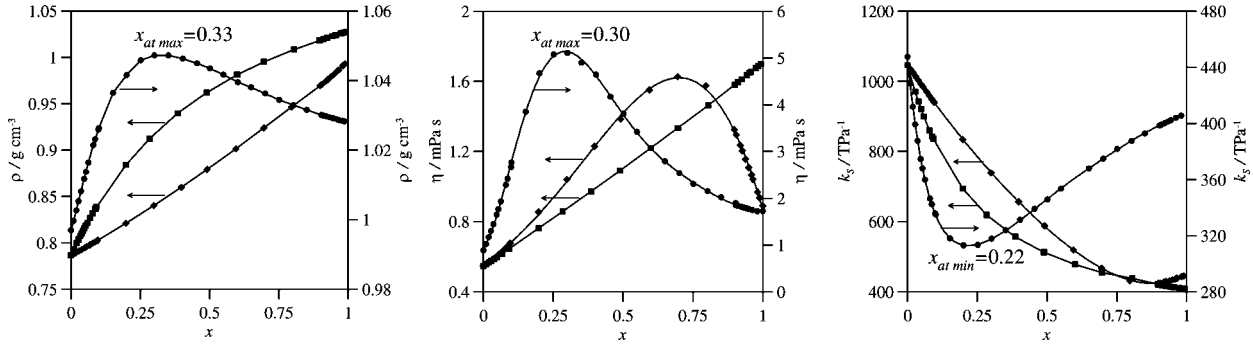

Figure 5. Density, ρ, dynamic viscosity, η, and isentropic compressibility, k_S, for (●) x NMP + (1 − x) W, (■) x NMP + (1 − x) M and (◆) x W + (1 − x) M at 298.15 K and 0.1 MPa. Symbols: experimental data. Lines: fitting curves with coefficients from Table S3 (Supporting Information).

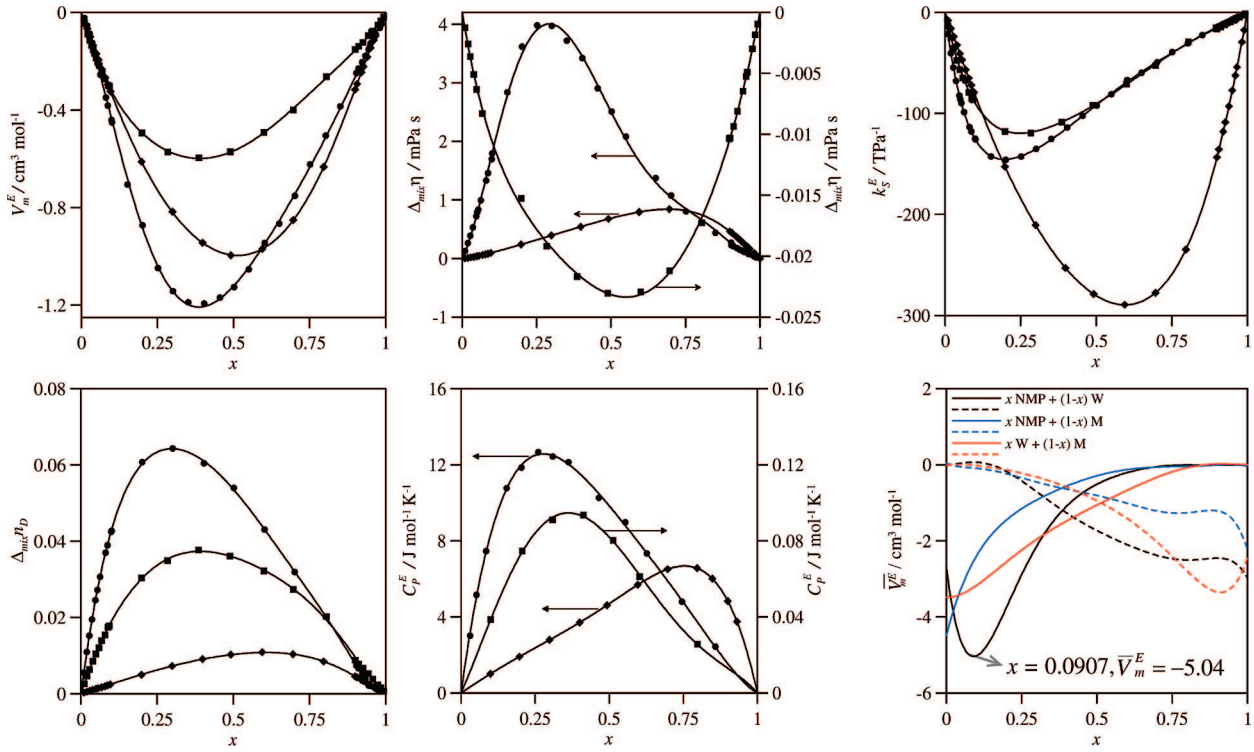

Figure 6. Excess and mixing properties for (●) x NMP + (1 − x) W, (■) x NMP + (1 − x) M and (◆) x W + (1 − x) M at 298.15 K and 0.1 MPa. Molar excess volume, V_m^E, mixing viscosity, $\Delta_{mix}\eta$, mixing refractive index, $\Delta_{mix}n_D$, excess isentropic compressibility, k_S^E, molar excess isobaric heat capacity, C_P^E, and partial molar excess volume of i-compound, $V_{m,i}^E$. Symbols: experimental data; lines: fitting curves with coefficients from Table S3 (Supporting Information).

internal platinum resistance thermometers (±1 × 10^{-2} K). The apparatus was calibrated using the density of *n*-nonane (Fluka, purity > 99.5%) and toluene (Sigma-Aldrich, purity > 99.5%) as standards.[20]

Dynamic viscosities (η) were measured using an Anton Paar AMV200 rolling ball microviscometer whose temperature was controlled using a Julabo F25 external thermostat and measured through a platinum resistance thermometer (±1 × 10^{-2}). The rolling time was measured to ±0.01 s with a stated precision in dynamic viscosity of ±5 × 10^{-3} mPa s. Calibration was performed using *n*-dodecane (Aldrich,>99.5%), hexan-1-ol (Fluka,>99.5%), octan-1-ol (Fluka,>99.5%), and decan-1-ol (Fluka, > 99.5%) as standards.

Refractive indexes (n_D) were measured to ±5× 10^{-6} with an automated Leica AR600 refractometer. The temperature was controlled by a Julabo F32 external circulator and measured through a platinum resistance thermometer (±1 × 10^{-2} K); the calibration was performed using water and a standard oil (n_D = 1.51416) supplied by the manufacturer.

Isobaric molar heat capacities (C_P) were measured to ±1 × 10^{-2} J mol^{-1} K^{-1} using a Setaram micro DSC III calorimeter. It consists of two vessels (reference and measuring) lodged in a calorimetric block surrounded by a thermostatic liquid (*n*-undecane) which ensures a constant temperature (±1 × 10^{-2}) controlled by peltiers. The measuring procedure is based on Calvet's principle, which determines the variation in the heat flow from/to the liquid sample upon the temperature scanning; measurements were performed according to the isothermal step method.[26] Hexane (Fluka, >99.5%) was the reference material and butan-1-ol (Aldrich,>99.5%) the calibration liquid whose C_P values were used for calibration.[19]

Molar excess volumes (V_m^E), mixing viscosities ($\Delta_{mix}\eta$), and mixing refractive indices ($\Delta_{mix}n_D$) were evaluated from the experimental readings according to the expressions reported earlier.[27] Isentropic compressibilities (k_S), were calculated from Laplace equation, and excess isentropic compressibilities (k_S^E) and molar excess isobaric heat capacities (C_P^E) according to the ideal behavior criterion.[28] The excess and mixing properties for

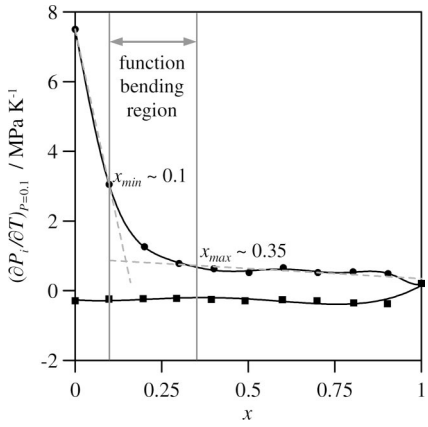

Figure 7. Temperature coefficient of internal pressure at 298.15 K and 0.1 MPa, $(\partial P_i/\partial T)_{P=0.1}$, for (●) x NMP + $(1-x)$ W, (■) x NMP + $(1-x)$ M calculated from data in refs 55 and 57. Gray dashed lines show the two linear regions, gray vertical lines show the function bending region beginning at x_{min} and finishing at x_{max}. Symbols: calculated from experimental data. Black continuous lines: trend lines for guiding purposes.

TABLE 1: Energy Change ($\Delta E = E_{solution} - E_{gas}$), Solvation Free Energies (ΔG_{sol}) and Electrostatic (ΔG_{elec}) and Non-Electrostatic ($\Delta G_{non\text{-}elec}$) Contributions to the ΔG_{sol} Calculated at B3LYP/6-311++g Theoretical Level in W and M Solutions (IEF-PCM) for NMP, with Energies in kcal mol^{-1}**

	ΔE	ΔG_{elec}	$\Delta G_{non\text{-}elec}$	ΔG_{sol}
water	−7.82	−8.18	7.07	−1.11
methanol	−7.53	−8.16	3.30	−4.86

TABLE 2: Infinite Dilution Partial Molar Excess Volume, $\bar{V}_m^{E,\infty}$, and Infinite Dilution Partial Molar Excess Isobaric Heat Capacity, $\bar{C}_P^{E,\infty}$, for x NMP + $(1-x)$ W, x NMP + $(1-x)$ M and x W + $(1-x)$ M at 298.15 K and 0.1 MPa

	$V_m^{E,\infty}$/cm^3 mol^{-1}		$C_P^{E,\infty}$/J mol^{-1} K^{-1}	
	1	2	1	2
(1) NMP + (2) W	−2.6827	−2.9804	115.75	14.01
(1) NMP + (2) M	−4.5982	−2.2825	0.36	0.18
(1) W + (2) M	−1.1556	−1.1242	28.43	69.89

the binary constituents (X^E) were correlated with composition, x, using the Redlich−Kister equation:[29]

$$X^E = x(1-x)\sum_{j=1}^{k} A_j(2x-1) \quad (1)$$

The values of the A_j coefficients were obtained by a least-squares procedure, and the optimum number of coefficients, k, were determined by an F-test.[30] The ternary excess and mixing properties (X_{TER}^E) were fitted to Cibulka equation[31]

$$X_{TER}^E = X_{BIN}^E + x_1x_2x_3(B_0 + B_1x_1 + B_2x_2) \quad (2)$$

where X_{BIN}^E represents the sum of the particular property for the three binary constituents deduced with eq 1; the last term in eq 2 is the so-called ternary contribution to the corresponding property. Tables S2−S6 (Supporting Information) collect the properties measured for the binary and ternary systems along with the fitting coefficients for the excess and mixing properties.

Molecular Modeling. To elucidate the strength and geometry features of the intermolecular forces in the ternary system, DFT computations of the NMP component and the NMP/W and NMP/M constituents were carried out in the gas phase and in solution. The DFT calculations were performed with the Gaussian 03 package,[32] using the Becke gradient corrected exchange[33] and Lee−Yang−Parr correlation[34] functionals with three parameters (B3LYP)[35] method. Full description of the electrons far from and close to the nuclei requires use of large and flexible basis sets, here the 6-311++g**. The atomic charges were calculated to fit the electrostatic potential[36] according to the Merz−Singh−Kollman (MK) scheme,[37] the fitting procedure being constrained to reproduce the whole molecular dipole moment. Calculations for the monomers and complexes in solution were carried out using the self-consistent reaction field (SCRF) approach; the solvent was treated as a continuum using the integral equation formalism of the PCM approach (IEF-PCM).[38] In the IEF-PCM approach the solute was placed in a cavity built using the united atom model; a value of 1.2 was used to scale all the radii and 70 tesserae to split the spherical surface. The torsional barriers were calculated by stepwise relaxed scanning of the potential energy surfaces in 10° intervals; in this scanning procedure the structure was fully optimized at every torsional angle step for the remaining degrees of freedom. The energy of the complexes was evaluated as the difference in energy between the complex and the monomer energies, the basis set superposition error (BSSE) being corrected according to the counterpoise procedure.[39]

To shed light on the structural dipole moment effects, classical molecular dynamics simulations of pure liquid NMP were carried out at 298.15 K and 0.1 MPa using the TINKER modeling package[40] in the NPT ensemble; the temperature and pressure of the simulation system was controlled with the Nosé-Hoover method.[41] The motion equations were solved using the Verlet Leapfrog integration algorithm.[42] Long-range electrostatic interactions were treated with the smooth particle mesh Ewald method.[43] The simulated infinite system consists of a cubic box with 250 NMP molecules to which periodic 3-directional boundary conditions were applied; the initial box size was set up according to the experimental densities. The simulations were performed using a $L/2$ Å cutoff radius for non bonded interactions, L being the initial box side. The initial boxes generated using the PACKMOL program[44] were minimized according to the MINIMIZE program in TINKER package to a 0.01 kcal mol^{-1} Å^{-1} rms gradient, and then several heating and quenching steps in the NVT ensemble were performed up to 500 K; likewise, a 100 ps NVT equilibration molecular dynamics simulation was run at each temperature. Finally, from the output of the NVT simulation configuration, 500 ps (time step 1 fs) were run in the NPT ensemble at the studied pressure and temperature; the first 100 ps were used to ensure equilibration (checked through constant energy) and the remaining 400 ps were stored. NMP was described according to the so-called optimized potential for liquid simulations, all atom version (OPLS-AA).[45] MK charges obtained through B3LYP/6-311++g** calculations were used in the simulations.

Kirkwood−Buff Analysis. The so-called Kirkwood−Buff integrals (KBI), G_{ij},[14a] may be calculated as:

$$G_{ij} = \int_0^\infty (g_{ij} - 1)4\pi r^2 \, dr \quad (3)$$

where g_{ij} stands for the radial distribution function of the species i around the central molecule j, and r is the separation distance between the centers of the two molecules. After the inversion was put forward by Ben Naim,[14b] the calculation of KBIs through three macroscopic thermodynamic properties (isothermal compressibility, activity coefficients and partial molar volumes) provides a fair link between the macroscopic and microscopic views. The partial molar volumes for the ternary mixture and the binary constituents are reported in this work.

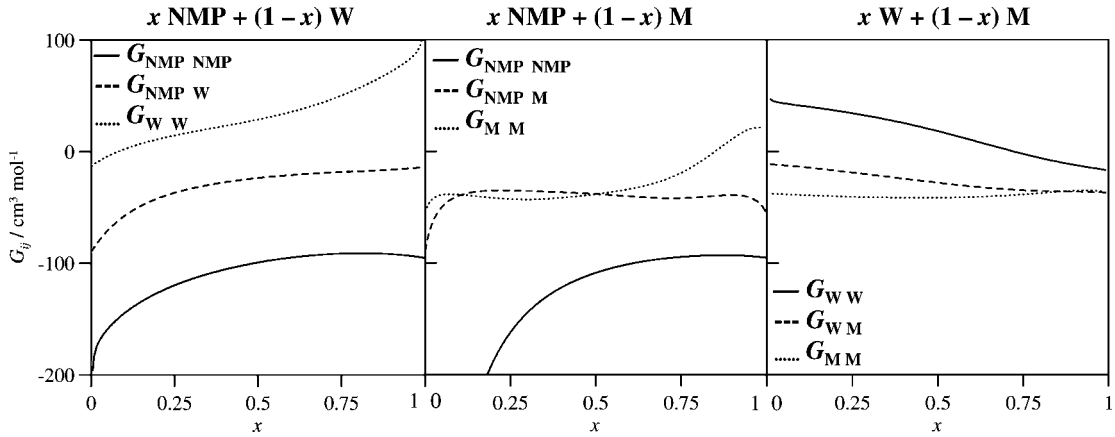

Figure 8. Kirkwood−Buff integrals, G_{ij}, for the reported binary systems calculated according to the inverted KB theory at 298.15 K and 0.1 MPa.

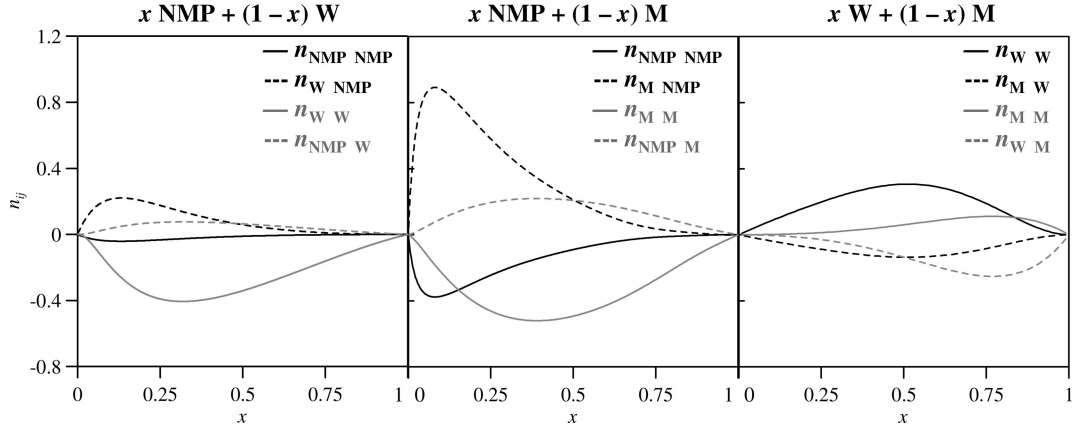

Figure 9. Excess of deficiency of molecules around a central *j*-one, $n_{ij,}$ in the reported binary systems calculated according to the inverted KB theory at 298.15 K and 0.1 MPa.

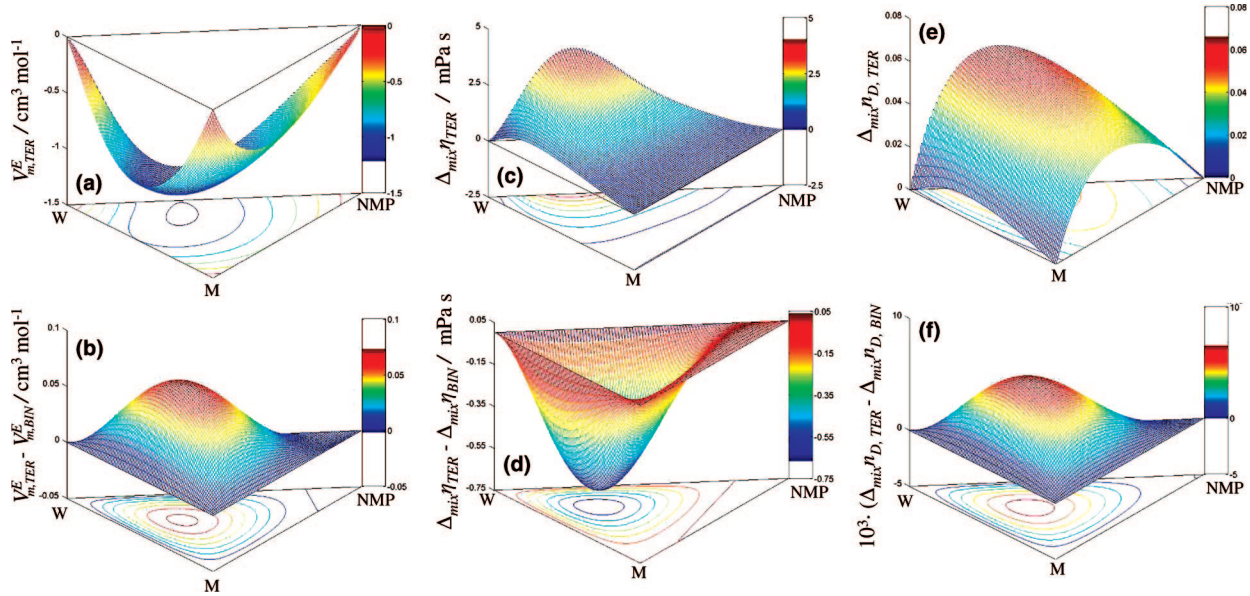

Figure 10. Molar excess volume, $V^E_{m,\ TER}$, ternary contribution to molar excess volume, $V^E_{m,\ TER} - V^E_{m,\ BIN}$, mixing viscosity, $\Delta_{mix}\eta_{TER}$, and ternary contribution to mixing viscosity, $\Delta_{mix}\eta_{TER} - \Delta_{mix}\eta_{TER}$, mixing refractive index, $\Delta_{mix}n_{D,TER}$, and ternary contribution to mixing refractive index, $\Delta_{mix}n_{D,TER} - \Delta_{mix}n_{D,BIN}$, for the x_1 NMP + x_2 W + $(1 - x_1 - x_2)$ M ternary system at 298.15 K and 0.1 MPa.

The isothermal compressibility contribution to G_{ij} is almost negligible,[46] therefore they were regarded as ideal and determined from the literature values for pure components.[7,21] To properly determine the partial derivatives of the chemical potential, the activity coefficients and their concentration dependence are needed. Unfortunately these were not experimentally available for all the systems studied; therefore, we had to fall back on the Dortmund UNIFAC[47] group contribution method applied previously.[48] The symmetrical ideal reference level suggested by Matteoli,[49] G_{ij}^{IDEAL}, was used to extract

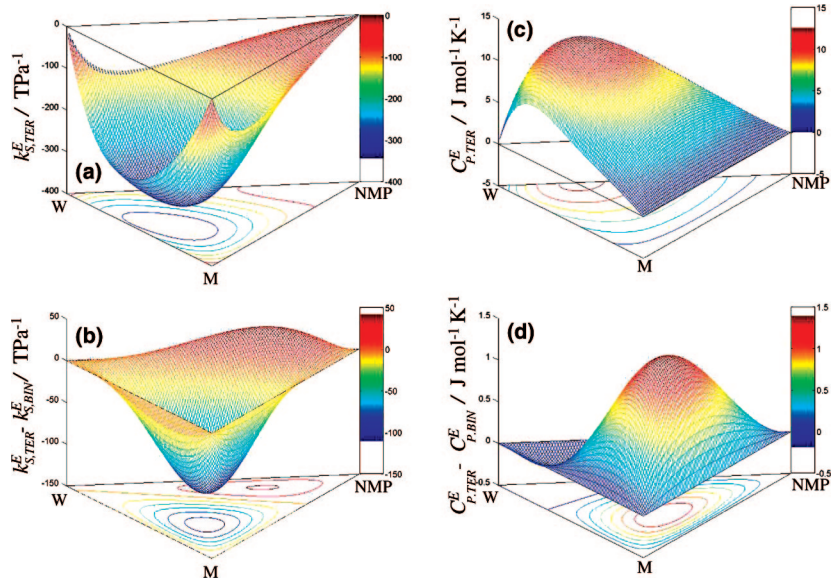

Figure 11. Excess isentropic compressibility, $k^{E}_{S,TER}$, and ternary contribution, $k^{E}_{S,TER} - k^{E}_{S,BIN}$, excess isobaric molar heat capacity, $C^{E}_{P,TER}$, and ternary contribution, $C^{E}_{P,TER} - C^{E}_{P,BIN}$, for the x_1 NMP + x_2 W + (1 − x_1 − x_2) M ternary system at 298.15 K and 0.1 MPa.

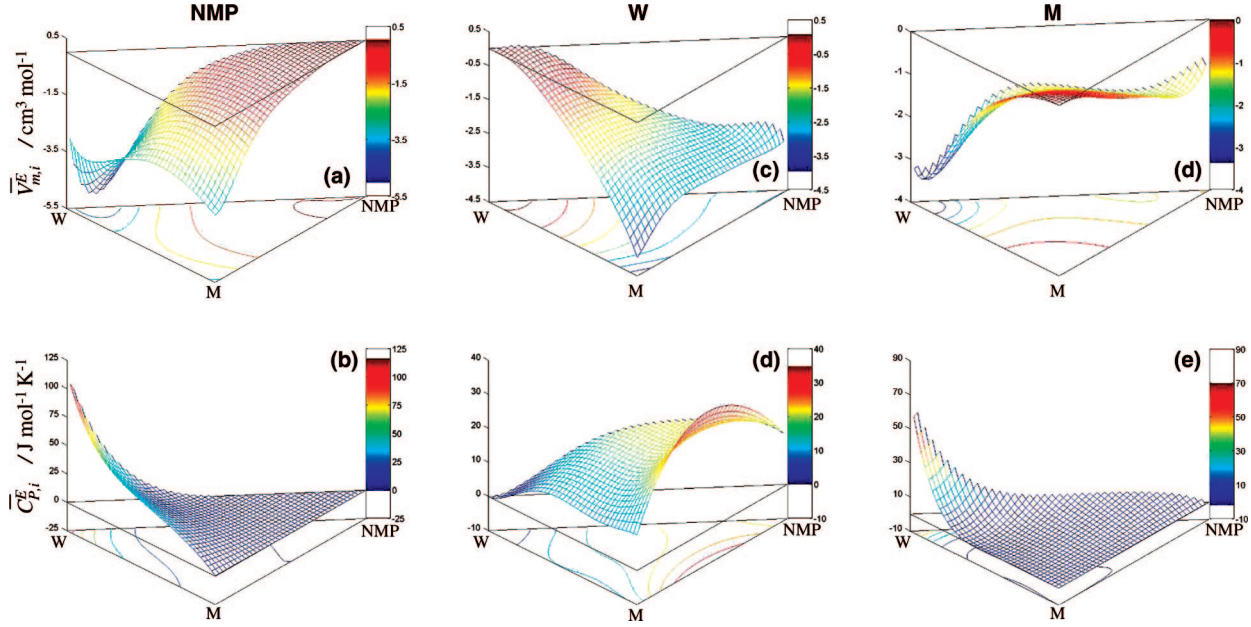

Figure 12. Partial molar excess volume of the *i*-compound, \overline V $^{E}_{m,i}$, and partial molar excess isobaric heat capacity, $\bar{C}^{E}_{P,i}$, in the x_1 NMP + x_2 W + (1 − x_1 − x_2) M ternary system at 298.15 K and 0.1 MPa. On top is indicated the mixture component for which the partial molar property is represented.

conclusions at molecular level on preferential solvation. Thus, the excess (or deficit) number of molecules around a central one, n_{ij}, can be calculated from the KBIs according to:

$$n_{ij} = c_i(G_{ij} - G_{ij}^{IDEAL}) \quad (4)$$

Here c_i is the concentration of the component *i*. To simplify the analysis, the ternary system was treated as a pseudobinary, that is, assuming constant mole fraction for one component and variable composition for the other two. Therefore, the ternary system was split into three pseudobinaries: x_1 (NMP) = 0.1, x_2 (W) = 0.1, and x_3 (M) = 0.1.

Results and Discussion

Computations on Pure NMP and NMP/W and NMP/M. DFT computations may afford valuable information on the NMP structure and the viability and strength of the H-bonding complexes with W and M as well. Figure 1 displays the gas phase results for pure NMP at the B3LYP/6-311++g**, and Table S7 (Supporting Information) those in the gas phase and W and M solutions. A considerable dipole moment, both in gas phase and in solution, was obtained for NMP directed from the carbonyl group across the ring; the liquid and gas-phase values are close together,[11] but those in W and M solutions clearly rose by some 40%. Concurrent with previous lower-level results for solid-phase and theoretical calculations,[50] the gas-phase NMP ring is not fully planar (Figure 1a), nor is it in solution (see dihedrals (11,2,3,1) and (3,2,11,10) Table S7, Supporting Information) clearly deviate from the 0° planar ring value. The (1, 10, 11, 2) dihedral around the amide bond shows the least deviations. A DFT analysis of the results shows a low ring puckering frequency at 156.6 cm^{-1}, in close agreement with the experimental 154

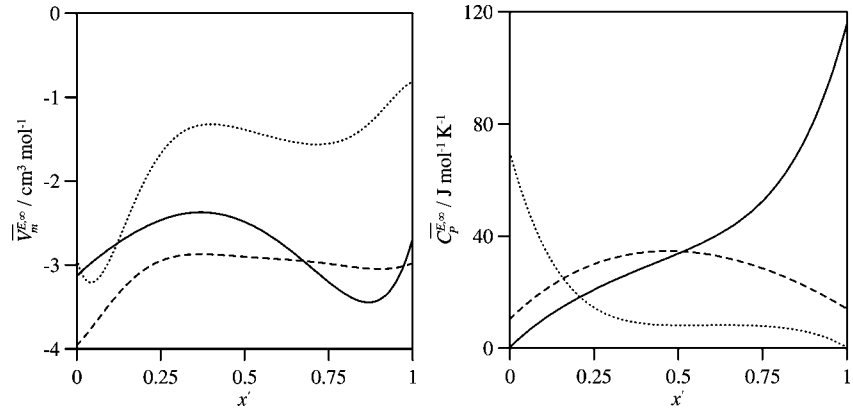

Figure 13. Infinite dilution partial molar excess volume, $\bar{V}_m^{E,\infty}$, and infinite dilution partial molar excess isobaric heat capacity, $\bar{C}_P^{E,\infty}$, in the x_1 NMP + x_2 W + $(1 - x_1 - x_2)$ M ternary system at 298.15 K and 0.1 MPa. (—) Values for NMP, as a function of x' W + $(1 - x')$ M with $x_{NMP} \rightarrow 0$; (--) values for W, as a function of x' NMP + $(1 - x')$ M with $x_W \rightarrow 0$; (•••) values for M, as a function of x' NMP + $(1 - x')$ M with $x_M \rightarrow 0$.

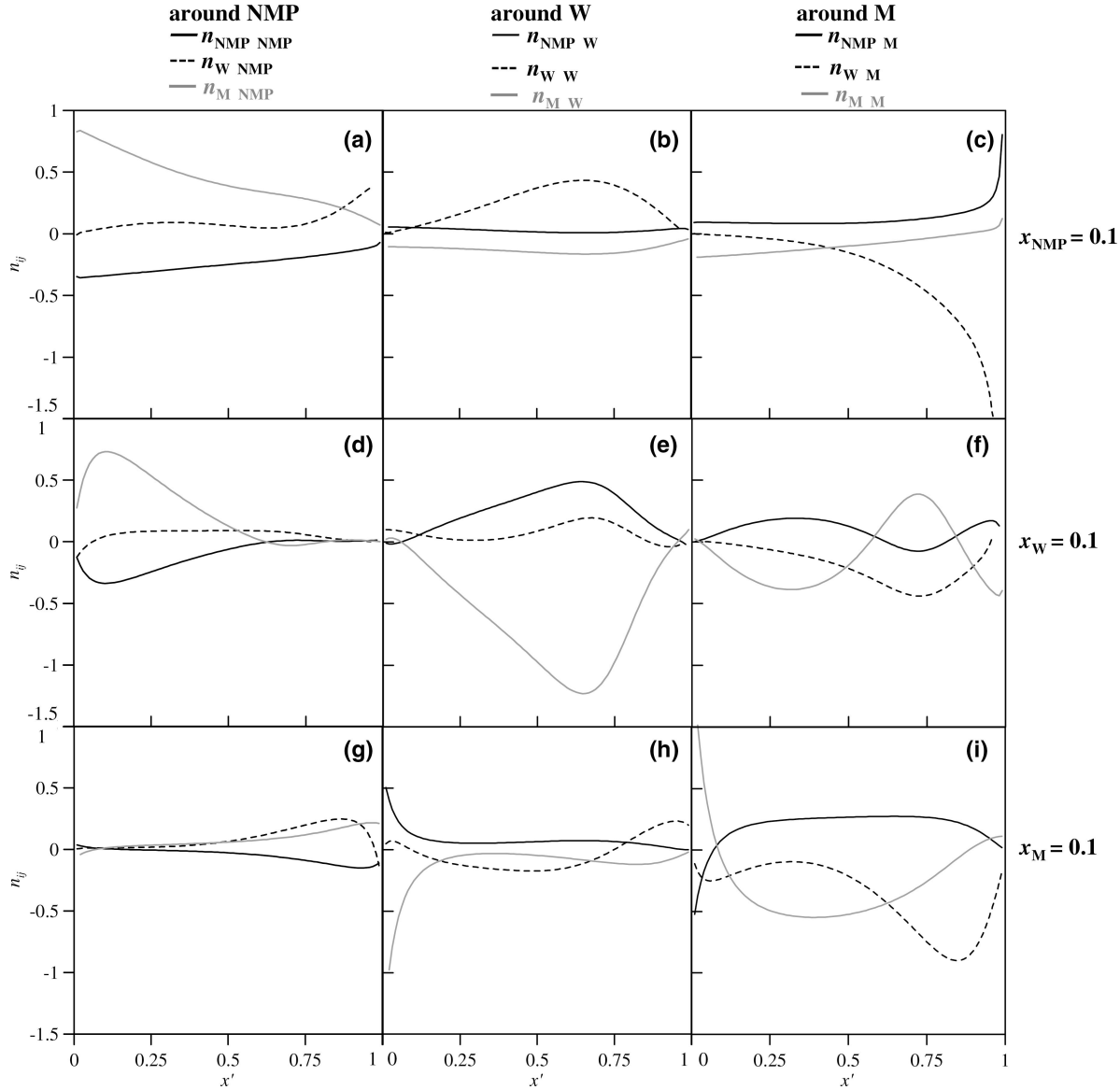

Figure 14. Excess of deficiency of molecules around a central one, $n_{ij,}$ in the pseudobinary systems x_1 NMP/ x_2 W/ x_3 M with constant $x_1 = 0.1$ (first row), $x_2 = 0.1$ (second row) and $x_3 = 0.1$ (third row), calculated according to the inverted KB theory at 298.15 K and 0.1 MPa. $x' = x_i/(x_i + x_j)$ where i and j are the mixture compounds with variable composition ($i = 2$ and $j = 3$ for first row; $i = 1$ and $j = 3$ for second row; $i = 1$ and $j = 2$ for third row).

cm^{-1},[51] pointing to fluctuations around the amide bond in gas-phase and also in solution.

Another important feature is the orientation of the NMP methyl group attached to the amide nitrogen. The (1,10,13,15)

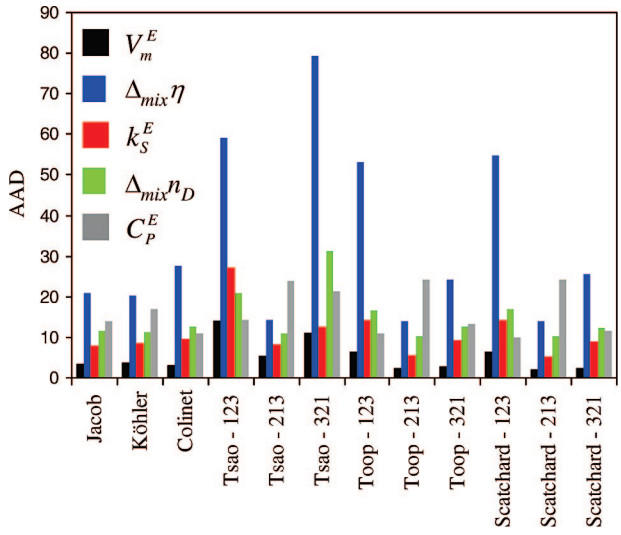

Figure 15. Absolute average deviation, AAD, for the predictions obtained with semiempirical models for the x_1 NMP + x_2 W + (1 − x_1 − x_2) M ternary system at 298.15 K and 0.1 MPa; for asymmetric equations the component 1 is (123) NMP, (213) W, and (321) M.

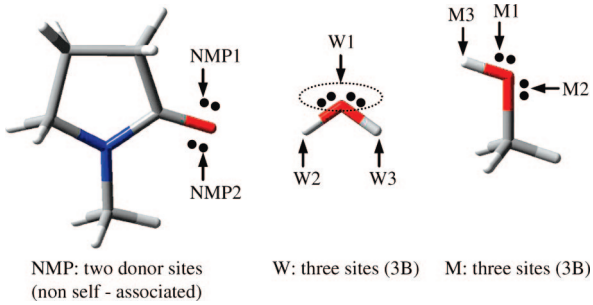

Figure 16. Schematic plot of association sites for the studied molecules. Dots represent lonely electron pairs.

dihedral angle (Table S7, Supporting Information) is close to 180° and that (11,10,13,15) slightly deviates from 0°; therefore, the preferred configuration of the methyl group involves a hydrogen atom almost eclipsing the CO oxygen, in contrast with the preferred staggered configuration in solid phase.[50] The positive charge borne by H(15) (Figure 1a) is fairly higher than that of the other hydrogen atoms, that is, the eclipsed configuration can be stabilized by the interaction between H(15) and the strongly negative CO oxygen, separated from one another by only 2.45 Å; this feature is borne out by the electrostatic potential surface (ESP) (Figure 1b), in which a continuity between negative (around the oxygen) and positive (around the hydrogen) regions is established. The potential energy scans for the rotational barriers around that methyl group (Figure 2) reveal that the eclipsed configuration is clearly preferred over the staggered one, with lower electrostatic O/H interaction. The modest gas-phase rotational barrier (1.30 kcal mol^{-1}), which drops in W and M solutions, is in close agreement with 1.2 kcal mol^{-1} reported at a lower theoretical level.[50]

Unlike the (11,12) CO bond, the (10,11) amide bond in solution is shorter than in gas phase, concurrent with the reinforcement of the negative charge at the CO oxygen site and with the dipole moment rise from gas-phase to solution; this feature is accounted for by the interaction between the large electron density on O (Figure 1, parts b and c) and the self-consistent reaction field, which has a tendency to separate the oxygen from the remaining moiety; this effect has been reported for other amides.[52] To accomplish the main objective of this work, the solution properties of NMP, the energy difference from gas-phase to W and M solutions, along with the free solvation energies, have also been calculated according to the PCM approach. Although the extent of stabilization in W and M solutions are similar, the solvation free energy in M is higher because of the higher nonelectrostatic contribution in M and the larger building cavity contribution in W; this feature can be related to the less compact structure of M, which fits better the NMP molecules.

An analysis of the molecular level structure of pure liquid NMP is also carried out by classical molecular simulations in the NPT ensemble. The site−site radial distribution functions (RDFs) for selected pairs (Figure 3) reveal a fluid structure characterized by marked dipolar ordering, that is, the (O−O) and (N−N) RDFs display broad peaks with maxima at 6.0 Å and first valleys at 8.2 Å, integrating to 4.9 and 4.6 molecules, respectively. The (O−H) RDF shows a low maximum at 2.9 Å probably ascribable to a feeble trend to H-bonding both sites, though the separation is too long for such an effect be remarkable. 1:2 NMP:W or 1:2 NMP:M complexes have been optimized in gas-phase and in their respective solutions (Figure 4). These aggregates show H-bonding with intermolecular distances remarkably low and the angles close to 120° decreasing in solution. The H-bond strength drops remarkably from gas-phase to solution, the values for W complexes being slightly stronger because of the building cavity energy contribution in the PCM model.

Properties of NMP/W, NMP/M and W/M Binary Constituents. Figure 5 and 6 display the thermophysical measurements and the derived excess and mixing properties, respectively. The three binary constituents clearly deviate from ideality. The NMP/W binary fully differs from the other two; the density, dynamic viscosity and isentropic compressibility values, with well defined maximum or minimum at NMP mole fraction around 0.3 (slightly lower for k_S, Figure 5), point to a very efficient NMP packing in the W H-bonding network, and favors 1:2 NMP:W heteroassociations, as DFT has revealed. The marked negative excess volume and excess isentropic compressibility and the positive mixing viscosity bear out the efficient packing and the complex formation. These results concur with the strong exothermic NMP/W mixing (excess enthalpy H^E = −2744 J mol^{-1} for x_{NMP} = 0.33 at 298.15 K).[53] The highly positive isobaric excess heat capacities (Figure 6 and data from Vasilev et al.)[54] with a maximum at 0.3 mol fraction, also point to a meaningful association. The partial molar excess volumes (Figure 6) give out a complex behavior; the NMP minimum at x_{NMP} = 0.09 defines a two-region scheme for mole fractions above and below this limit. These features concur well with the internal pressures reported earlier.[55] At low NMP mole fraction this property rises with the temperature rise, as occurs with systems with marked H-bonding networks; however, at high NMP concentration it is almost temperature independent. The composition effect on the temperature coefficients of internal pressure may be saved to analyze the mixing scheme in Figure 7, where two linear stretches and a transition bending region are obtained.[56] The outset of the bending region corresponds to a mole fraction coincident with the minimum in the partial molar excess volume; the ending appears at a mole fraction close to the completion of the linear region after the minimum in the partial molar excess volume. Three regions can then be defined in this scheme: (I) $0 < x < 0.1$, (II) $0.1 < x < 0.35$, and (III) $x > 0.35$. Despite the low solvation energy, region I reflects that NMP nicely fits the water network (Table 1); the negative infinite dilution partial molar excess volume of NMP

TABLE 3: PC-SAFT Parameters and Absolute Average Deviations, AAD, for the Correlation of Saturation Properties of Pure Components[d]

	(ε/k)/K	σ/Å	m	(ε^{AB}/k)/K	κ^{AB}	AAD P^{sat}	AAD ρ_{liq}^{sat}	$T_{r,range}$	ref
NMP	310.57	3.3284	3.6758			6.65	0.09	0.38−0.50	*a*
W	327.62	2.4697	1.7960	1558.4	0.068277	0.87	6.36	0.42−0.98	*b*
M	160.65	2.3246	0.2586	1613.7	0.258600	2.15	1.22	0.41−0.98	*c*

[a] Reference 55. [b] References 68 and 69. [c] Reference . [d] $T_{r,range}$ = Reduced temperature range used for data correlation. W and M were modeled according to the three-site scheme in Figure 14.

TABLE 4: PC-SAFT Mixture Parameters from Correlation of Experimental Densities, ρ, for x NMP + $(1 - x)$ W, x NMP + $(1 - x)$ M and x W + $(1 - x)$ M at 298.15 K and 0.1 MPa[a]

	k_{12}	sites i, j	$(\varepsilon^{i,j}/k)$/K	$\kappa^{i,j}$	AAD ρ
NMP + W	−0.1421	i = NMP1, NMP2 j = W2, W3	1259.6	0.0995	1.44
NMP + M	0.0533	i = NMP1, NMP2 j = M3	1257.9	0.0775	1.17
W + M	0.0279	i = W1 j = M3	1301.3	0.0355	4.41
		i = W2, W3 j = M1, M2	1302.0	0.0475	

[a] i and j stand for the sites involved in each interaction according to Figure 14.

(Table 2) proves this feature, showing an effective hydrophobic and hydrophilic solvation. The large positive value of infinite dilution partial molar excess isobaric molar heat capacity points in the same direction. Region II commences with the minimum of partial molar excess volume; in this region occurs the most remarkable NMP effect on the W network; the water H-bonding rupture is counteracted by the formation of NMP/W heteroassociations, mainly 1:2 NMP:W, as the upper boundary of region II shows ($x_{NMP} \sim 0.35$, thus 1:2 NMP:W complexes). For region III the packing is less efficient and the W molecules are dispersed in the NMP structure probably forming 1:1 heteroassociations, as confirmed by the negative W partial molar excess volumes (Figure 6).

An analysis according to the inverted KB theory can shed light on the molecular level features. KBIs reported in Figure 8 show a monotonic trend. For NMP/W the most negative values, corresponding to $G_{NMP/NMP}$, reflect NMP/NMP dipole interactions, whereas NMP/W and W/W are H-bonding. A clear preferential solvation stems from the results in Figure 9. For NMP/W, the solvation spheres of NMP and W show a deficit of like molecules with excess of hetero molecules; this effect is pronounced at amide concentration $x_{NMP} < 0.3$, which points to 1:2 NMP:W complexes. As the NMP concentration is boosted, the preferential solvation diminishes and the water molecules appear dispersed in the NMP liquid structure.

The NMP/M behavior differs from that of NMP/W. The density, dynamic viscosity and isentropic compressibility plots show no maximum or minimum (Figure 5). The excess and mixing properties indicate that NMP/M behaves nonideally, but the deviations are much lower; likewise, the excess enthalpy values were four times lower than those for NMP/W ($H^E = -658$ J mol^{-1} for $x_{NMP} = 0.53$ at 298.15 K).[58] The maxima and minima for excess and mixing properties shift toward higher NMP content. The negative molar excess volume, the close to null mixing viscosity, the DFT computations and the exothermic nature, they all imply an efficient packing and NMP/M heteroassociations; these, in fact, are less but similar in strength to NMP/W (Figure 4). Also the data of Figure 7 reveal a fairly different behavior; the nearly constant temperature coefficient of internal pressure concurs with the observed trend of partial molar excess volume. The negligible partial molar excess isobaric heat capacity at infinite dilution for NMP in NMP/M points to the prevalence of geometry effects against heteroassociations. At high dilution, the negative partial molar excess volumes for M show the fair fitting in the NMP structure. The KB analysis shows marked preferential solvation compared to NMP/W, a larger M excess molecules in the NMP solvation sphere with a maximum at 0.1 mol fraction; although a slight NMP excess appeared in the M spheres, this is less marked, and at low amide content NMP nicely fits in the M H-bonding network. The larger M excess around a central NMP points to geometry effects that determine the solvation sphere structure; the larger M size and its well-known tendency to clustering hinders the presence of NMP in the neighborhood of a central NMP, thus raising the M excess in the NMP solvation sphere. Also for NMP/M the preferential solvation vanishes as the NMP content is boosted.

The maximum in dynamic viscosity observed for W/M (Figure 5) denotes a complex behavior. The negative excess volume and the isentropic compressibility both point to an efficient packing of the two components and the positive mixing viscosity and excess isobaric heat capacity to the existence of H-bonding heteroassociations (Figure 6). The proposed approach was probed using W/M mixtures to calculate KBIs;[48] a fair agreement with the literature data validated the KBIs calculation using UNIFAC. However, an analysis of the KBIs recently published for the W/M system shows remarkable differences;[59] some of these KBIs used inconsistent experimental data, mainly the vapor−liquid equilibrium data applied gave rise to deviations. The KBIs from Ruckenstein and Sulgin,[46] obtained through a rigorous analysis and selection of the experimental sources, yielded reliable KBIs used for comparative purposes.[48] Another possible controversy lies in the way of calculating the excess or deficit number of molecules around a central one. The reference ideal state used in this work, eq 4, has been discussed recently in particular for the W/M system;[60,61] The results obtained with eq 4[46] and those according to the new method proposed by Ruckenstein and Shulgin[61] (method 2) differ not only quantitatively but also qualitatively mainly for the solvation around M. The results of Figure 9c using eq 4 show that M is preferentially solvated by M molecules over the whole composition range; however, the results according to method 2 show that M is preferentially solvated by M molecules up to $x(M) = 0.35$, whereas for higher M contents surprisingly M molecules are preferentially solvated by W molecules. In other words, M is preferentially solvated by W in M-rich mixtures according to method 2. It is the authors belief that calculations according to eq 4 give rise to a more realistic physical picture than those from method 2. Recent soft-X-ray fluorescence spectroscopy studies[62] have shown the existence of bended M chains interacting with W forming open ring structures over the whole composition range. Thus, the molecular picture inferred from these results implies that M is preferentially surrounded by M molecules although W acts as

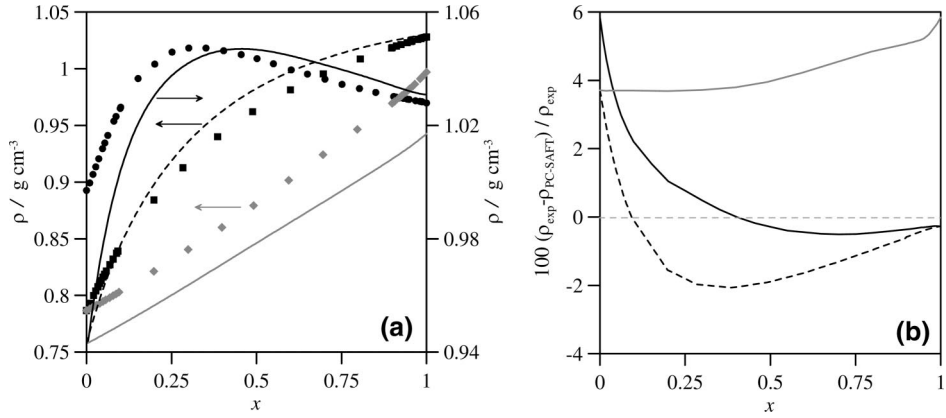

Figure 17. Experimental (symbols) and PC-SAFT (lines) densities, ρ, for (●,—; black) x NMP + $(1 - x)$ W, (■, --; black) x NMP + $(1 - x)$ M and (◆, —; gray) x W + $(1 - x)$ M at 298.15 K and 0.1 MPa. In part b are reported percentage deviations. Pure compound parameters from Table 3 and mixture parameters from Table 4were used.

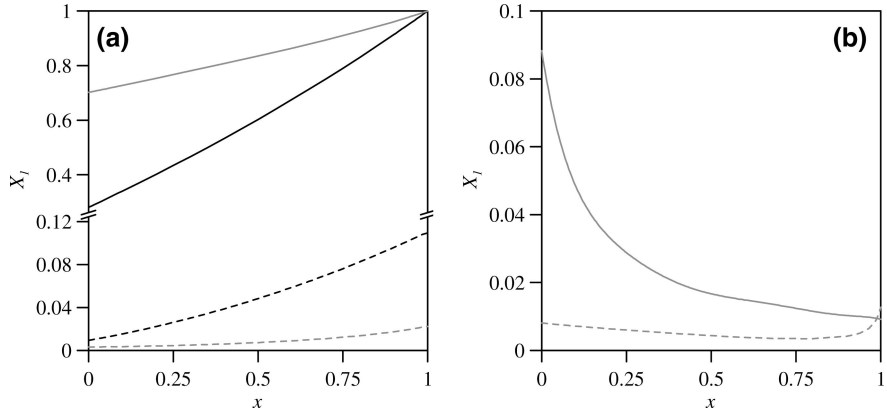

Figure 18. Monomer fraction, X_1, calculated from PC-SAFT model and Table 4 parameters for (black) x NMP + (1 - x) W, (gray in part a) x NMP + $(1 - x)$ M and (gray in part b) x W + $(1 - x)$ M at 298.15 K and 0.1 MPa. Continous lines: X_1 for first compound of the mixture. Dashed lines: X_1 for the second compound of the mixture.

a bridge; this concurs with the M excess around M obtained with eq 4 and disagrees with the results from method 2. Moreover, it is only hardly justifiable the M excess around M in the M-rich regions inferred from method 2, considering that even in the highly diluted region M tends to form large clusters.[63] Hence, the results from eq 4 should be regarded as reliable enough and then this method has been used further.

The H-bonding self-association affinity given away by the calculated KBIs (Figure 8) is larger for W compared to M, whereas the W/M heteroassociations show an intermediate behavior. Figure 9 shows a clear preferential solvation for W, that is, although W-M H-bonding is established, both molecules tend to be surrounded by like molecules.

Properties of the NMP/W/M Ternary System. The excess and mixing properties for the ternary system are plotted in Figures 10–13 The molar excess volumes were negative over the full composition range, with a minimum close to the NMP/W binary; addition of M gives rise to a feeble expansion (Figure 10b, and Table S6, Supporting Information). The partial molar excess volumes, negative throughout (Figure 12), bear out the good fitting among the three components; the even more negative values for NMP and W support the larger NMP/W affinity. The infinite dilution values (Figure 13) point out a better W fitting in the NMP/M mixture compared to the M fitting in the NMP/W mixture, that is, the NMP/W binary gives rise to a more efficient packing, but M can only hardly be accommodated. Likewise, NMP is properly accommodated in W/M mixtures, thereby the NMP affinity is greater for W than for M; these features support that NMP is H-bonded both with M and W, but with W the forces are prevalent, whereas for M it is the size effect that is prevailing. Therefore, the concurrence of W and M in the ternary mixture generates a looser packing where NMP, though fitting efficiently, hinders the growing of intermolecular interactions among the components. This observation is borne out by the mixing viscosities; although this property was positive throughout, the observed maximum corresponds to the NMP/W binary (Figure 10c) and a prominent negative ternary contribution is obtained (Figure 10d). In conclusion, H-bonding in the ternary system is loosed and both self-and hetero associations become tempered or even hindered compared with the binaries. The mixing refractive index was always positive; the maximum observed for the NMP/W binary confirms the loosening effect upon formation of the ternary mixture.

The excess isentropic compressibility was negative over the full composition range; the minimum close to the W/M binary (Figure 11a) is consistent with the most negative values for W/M (Figure 6). The negative ternary contribution (Figure 11b, Table S6, Supporting Information) supports the incompressible trend of this binary, reinforced by addition of small NMP amounts; for NMP-rich zones the positive ternary contribution reinforces the mixture compressibility upon addition of M, these features pointing to the hindering M effect on the mixture structure.

The excess isobaric heat capacity, positive throughout, evinces H-bonding forces; the maximum observed in the NMP/W axis endorses the force loosening upon addition of M. The ternary contribution shows a negative zone with a minimum in the M-poor region (meaning disruption of NMP/W interactions upon

addition of M), and a maximum in M-rich zones; these features get the message across that the fluid structure is mainly controlled by the M/M H-bonding network, which favors a proper fit of small M and NMP amounts rearing 1:1 heteroassociations. Partial molar excess heat capacities were positive for the three components (Figure 13); the highest values, concerned with NMP in W/M mixtures, increase as the W mole fraction is boosted and show the larger NMP/W affinity. The values for M decrease in NMP/W as the NMP mole fraction rises, pointing to hindering of NMP/M interactions in amide-rich regions. W shows an almost equal affinity for M and NMP, the partial molar heat capacity maximum, close to 0.5, showing that W can develop heteroassociations both with M and NMP.

For NMP-rich mixtures, addition of M disrupts both the self- and hetero H-bonding networks; although new associations are set up with M, these are either weaker or less due to the expansive effect arising from addition of M; on the contrary, if M is the major component, addition of NMP and W does not remarkably disrupt the less compact fluid structure and both components can be accommodated in the fluid structure rearing new interactions with M.

The Kirkwood−Buff analysis in the pseudobinary approach (Figure 14) proves the complexity of the ternary system. For low concentrations ($x_{NMP} = 0.1$) NMP is preferentially solvated by W and M, whereas W is preferentially solvated by W. At such low amide concentration, M shows no substantial preferential solvation, sustaining the larger NMP/W affinity; this feature is even more remarkable at low amide concentrations, where the 1:2 NMP:W hetero associations prevail. For low W mixtures ($x_W = 0.1$) the preferential W solvation around NMP disappears as the NMP concentration rises; although there is a rather small M excess in the NMP spheres, at low NMP concentrations M is preferentially surrounded by W but, as the amide concentration rises, the preferential solvation vanishes and W and M appear dispersed within the NMP-dominated dipolar liquid structure. At such high NMP concentrations, 1:1 NMP:W or NMP:M heteroassociations could be developed. At this NMP content, W is preferentially solvated by NMP as the NMP content rises, reflecting the picture of W molecules dispersed in the NMP network. M shows a somewhat less clear behavior; at low NMP concentrations, there is a slight deficit of M molecules in its solvation sphere, whereas at higher NMP concentrations a maximum appears. Finally, at $x_M = 0.1$, the most complex picture obtained shows that the M effect differs from the other two. In the NMP solvation sphere, a soft excess of W and M appears, in agreement with the W spheres composition; on the contrary, a slight deficit of W and M appears for the M solvation spheres. Thus, the KB analysis shows the fair NMP/W affinity. NMP and W are preferentially solvated by W and NMP, respectively, developing NMP/W heteroassociations. M, on the contrary, tends to be surrounded by W, stabilizing the H-bonding network; only at high NMP concentrations M is surrounded by the amide because M fits properly in the NMP-dominated liquid structure.

Semiempirical Modeling of Thermophysical Properties. Since experimental determinations often are only hardly attainable, quite a useful task comes from the need to predict properties for multicomponent systems from available binary data. An approach of broad appeal consists of semiempirical models that may afford reliable results, even though a deep theoretical basis is lacking.[15] These models may be classified as asymmetric, if they rely on the arbitrary numbering of the components, or else symmetric. The symmetric models by Jacob-Fitzner, Köhler, and Colinet, and the asymmetric ones by Tsao-Smith, Toop, and Scatchard have been tested;[15,64] Figure 15 shows the outcome for excess and mixing properties. The refinement of the predictions with the simpler symmetric models is low (especially for mixing viscosity) and similar to that with the more complex asymmetric. To reach lowest deviations with asymmetric models, numbering as 1 the common component of the two constituents with larger deviations from ideality (or from zero mixing property) is recommended; this compound should be W (Figure 6) and thus asymmetric models numbering 213 should provide lower deviations. This criterion has led to lower deviations for the three asymmetric models tested. The complex structure of the ternary system originated deviations above 5% for all properties and models and thus, this approach should be ruled out.

PC-SAFT Modeling. The PC-SAFT model,[16] successful in many instances, has attracted a great deal of interest both in industry and academia.[65] In this model a hard-chain reference fluid, derived by extending the perturbation theory to chain molecules,[66] is the reference for the EOS dispersion term. For nonassociating components, the model consists of three parameters: (i) the number of chain segments (m), (ii) the segment diameter (σ), and (iii) the potential depth (ε/k). For associating molecules two additional parameters are, in turn, required: (iv) the association volume (κ^{AB}) and (v) the association energy (ε^{AB}/k). To determine the segment-segment unlike dispersive interactions, the PC-SAFT is extended to mixtures using a simple parameter mixing rule, thereby only a single binary interaction parameter (k_{ij}) is required. The association scheme for each component, that is, the number of donor and acceptor H-bonding sites, most commonly is a priori defined; in this work NMP was regarded as non self-associative and W and M as three-site components, 3B according to Huang and Radosz (Figure 16).[67] M was modeled as a rigorous three-site molecule, and W was considered also as a three-site component since previous studies have shown this scheme to be more adequate than the more rigid four-site one.

NMP is unable to cause H-bonding self-associations but, when mixed with W or M, the two lone-pairs of electrons give rise to heteroassociations. Therefore, to apply PC-SAFT, the interaction energy between the NMP1 and NMP2 donor sites (Figure 16) and the W and M hydrogen atoms must be taken into consideration; these two energy parameters together with those arising from the W/M interaction were obtained by optimizing the experimental density data for the ternary system. Properties for pure components were obtained from correlation of saturation pressure and liquid density data (Table 3); NMP and M were nicely correlated, whereas for the W saturated liquid density the rather high deviations reveal a complex structure. Table 4 and Figure 17 show the PC-SAFT results for the binary constituents; although the model describes qualitatively the density curves, even the maximum reached for NMP/W mixtures, the data remarkably deviate from the experimental values, which decreased for the NMP systems as the NMP mole fraction was boosted. This feature can be justified by the complex H-bonding structure in the mixed fluid, where self- and hetero associations are present together with steric effects, not fully recruited by the model. The high density deviations for pure W (Table 3) are extended to W-containing mixtures, thus increasing the deviations. The model quantitatively predicts the nonideal behavior of the mixtures with only few parameters. The interaction parameters that account for the NMP/W/M hetero associations, strikingly high, point to NMP/W or NMP/M interactions. Application of PC-SAFT to NMP/W/M was carried out fully in a predictive way, thus only binary parameters were

considered and the absolute average deviation obtained, 3.5%, can be regarded as satisfactory considering the complex ternary effects in the mixture.

A main advantage of molecular-based EOS, such as PC-SAFT, is the unambiguous physical meaning the parameters convey, thus supplying information on fluids structure. An important property for H-bonded systems is the monomer fraction, X_1, defined as the nonassociating fraction molecules; the data plotted in Figure 18 show a marked association both with W and M, decreasing as the NMP concentration rises. At NMP-rich levels, W appears to interact with M less efficiently than M, although strong interactions are obtained for both components, as the low X_1 values show. The W/M system shows strong heteroassociation both in W and M rich regions.

Concluding Remarks

The NMP/W/M ternary system and their binary constituents strongly deviate from ideality, with marked effects arising from the competing self- and hetero H-bonding associations. NMP strongly interacts with W and M, but the disrupting effect on the W network is more remarkable; at low NMP concentration the NMP/W system suffers from noticeable interactions and preferential hetero solvation in the solvation spheres of both components. For NMP/M mixtures also the steric effects are important, but the interactions are less remarkable; although a certain preferential solvation is observed, that is not as clear as in NMP/W. The complexity of the ternary system is shown by the unsuccessful predictions the models provide and by the complex ternary contributions to the excess and mixing properties. PC-SAFT models nicely predict qualitatively the mixture properties, but the quantitative predictions were not fine enough.

Acknowledgment. Financial support by Junta de Castilla y León, Project BU-020A/07, and Ministerio de Education y Ciencia, Project CTQ2005-06611/PPQ (Spain), is gratefully acknowledged.

Supporting Information Available: Table S1 (thermophysical properties of pure solvents), Table S2 (calculated NMP parameters), Table S3 (binary properties), Table S4 (fitting coefficients for binary properties), Table S5 (ternary properties), Table S6 (fitting coefficients for ternary properties), and Table S7 (maxima and minima of ternary contributions to excess and mixing properties). This material is available free of charge via the Internet at http://pubs.acs.org.

References and Notes

(1) (a) Cox, K. R. *Fluid Phase Equilib.* 1993, *82*, 15; (b) Dorm, R.; Poll, O. *Fluid Phase Equilib.* 2002, 194−197, 15;(c) Harvey, A. H.; Alsace, A. *Chem. Eng. Prig.* **2002**, *98*, 34.

(2) (a) Prausnitz, J. M.; Lichtenthaler, R. N.; Gomes de Azevedo, E. *Molecular Thermodynamics of Fluid Phase Equilibria*, Prentice-Hall, New York, 1986. (b) Hansen, J. P.; McDonald, I. R. *Theory of Simple Liquids*; Academic Press: San Diego, CA, 2006. (c) Marcus, Y. *Solvent Mixtures: Properties and Selective Solvation*; Marcel Dekker: New York, 2002.

(3) (a) Archer, W. L. *Industrial Solvents Handbook*; Marcel Dekker: New York, 1996. (b) Reichardt, C. *Solvents and Solvent Effects in Organic Chemistry*; Wiley-VCH: Weinheim, Germany, 2003.

(4) Chen, C. C.; Mathias, P. M. *AIChE J.* **2002**, *48*, 194.

(5) (a) Raal, J. D.; Muhlbauer, A. L. *Phase Equilibria. Measurement and Computation*; Taylor & Francis: Philadelphia, PA, 1998; (b) Wakeham, W.; Assael, M. J. In *Chemical Thermodynamics for Industry*; Letcher, T. M., Ed.; Royal Society of Chemistry: London, 2004.

(6) (a) Kazantzi, V.; Qin, X.; El-Halwagi, M.; Eljack, F.; Eden, M. *Ind. Eng. Chem. Res.* **2007**, *46*, 3400. (b) Eljack, F. T.; Eden, M. R.; Kazantzi, V.; Qin, X.; El-Halwagi, M. M. *AIChE J.* **2007**, *53*, 1232.

(7) Hradetzky, G., Hammerl, I.; Bittrich, H. J.; Wehner, K.; Kisan, W. *Selective Solvents. Physical Sciences Data 31*; Elsevier: Amsterdam, 1989.

(8) Linek, J.; Wichterle, I.; Marsh, K. N. *J. Chem. Eng. Data* **1996**, *41*, 1212.

(9) Lee, K. P.; Chromey, N. C.; Culik, R.; Barnes, R. J.; Schneider, P. W. *Fundam. Appl. Toxicol.* **1987**, *9*, 222.

(10) Chow, S. T.; Ng, T. L. *Water Res.* **1983**, *17*, 117.

(11) Fischer, E. *J. Chem. Soc.* **1955**, 1382.

(12) Fischer, K.; Gmehling, J. *Fluid Phase Equilib.* **1996**, *119*, 113.

(13) (a) Noll, O.; Fischer, K.; Gmehling, J. *J. Chem. Eng. Data* **1996**, *41*, 1434. (b) Henni, A.; Hromek, J. J.; Tontiwachwuthikul, P.; Chakma, A. *J. Chem. Eng. Data* **2004**, *49*, 231.

(14) (a) Kirkwood, J. G.; Buff, F. P. *J. Chem. Phys.* **1951**, *19*, 774. (b) Ben Naim, A. *J. Chem. Phys.* **1977**, *67*, 4884.

(15) Acree, W. E. *Thermodynamic Properties of Nonelectrolyte Solutions*; Academic Press: New York, 1984.

(16) (a) Gross, J.; Sadowski, G. *Ind. Eng. Chem. Res.* **2001**, *40*, 1244. (b) Gross, J.; Sadowski, G. *Ind. Eng. Chem. Res.* **2002**, *41*, 5510.

(17) Yang, C.; Xu, W.; Ma, P. *J. Chem. Eng. Data* **2004**, *49*, 1794.

(18) Blanco, B.; Sanz, M. T.; Beltrán, S.; Cabezas, J. L. *J. Chem. Eng. Data* **2002**, *47*, 1167.

(19) Zabransky, M.; Ruzicka, V.; Mayer, V.; Domalski, E. S. *J. Phys. Chem. Ref. Data Monogr.* **1996**, 6.

(20) http://webbook.nist.gov/chemistry/.

(21) Riddick, J. A.; Bunger, W. B.; Sakano, T. K. *Organic Solvents Physical Properties and Methods of Purification*; Wiley: New York, 1986.

(22) Nakamura, M.; Tamura, K.; Murakami, S. *Thermochim. Acta* **1995**, *253*, 127.

(23) Canosa, J.; Rodríguez, A.; Tojo, J. *J. Chem. Eng. Data* **2000**, *45*, 471.

(24) Resa, J. M.; González, C.; Ortiz, S.; Lanz, J. *J. Chem. Eng. Data* **2002**, *47*, 1123.

(25) Alcalde, R.; Aparicio, S.; García; B.; Dávila, M. J.; Leal, J. M. *New J. Chem.* **2005**, *29*, 817.

(26) Cerdeiriña, C. A.; Migues, J. A.; Carballo, E.; Tovar, C. A.; de la Puente, E.; Romaní, L. *Thermochim. Acta* **2000**, *347*, 37.

(27) García, B.; Alcalde, R.; Aparicio, S.; Trenzado, J. L.; Leal, J. M. *Ind. Eng. Chem. Res.* **2003**, *42*, 920.

(28) Benson, G. C.; Kiyohara, O. *J. Chem. Thermodyn.* **1979**, *11*, 1061.

(29) Redlich, O.; Kister, T. *Ind. Eng. Chem.* **1948**, *40*, 345.

(30) Bevington, P. *Data Reduction and Error Analysis for the Physical Sciences*; McGraw-Hill: New York, 1969.

(31) Cibulka, I. *Collect. Czech. Chem. Commun.* **1982**, *47*, 1414.

(32) Frisch, M. J. ; Trucks, G. W.; Schlegel, H. B.; Scuseria, G. E.; Robb, M. A.; Cheeseman, J. R.; Montgomery,Jr., J. A.; Vreven, T.; Kudin, K. N.; Burant, J. C.; Millam, J. M.; Iyengar, S. S.; Tomasi, J.; Barone, V.; Mennucci, B.; Cossi, M.; Scalmani, G.; Rega, N.; Petersson, G. A.; Nakatsuji, H.; Hada, M.; Ehara, M.; Toyota, K.; Fukuda, R.; Hasegawa, J.; Ishida, M.; Nakajima, T.; Honda, Y.; Kitao, O.; Nakai, H.; Klene, M.; Li, X.; Knox, J. E.; Hratchian, H. P.; Cross, J. B.; Adamo, C.; Jaramillo, J.; Gomperts, R.; Stratmann, R. E.; Yazyev, O.; Austin, A. J.; Cammi, R.; Pomelli, C.; Ochterski, J. W.; Ayala, P. Y.; Morokuma, K.; Voth, G. A.; Salvador, P.; Dannenberg, J. J.; Zakrzewski, V. G.; Dapprich, S.; Daniels, A. D.; Strain, M. C.; Farkas, O.; Malick, D. K.; Rabuck, A. D.; Raghavachari, K.; Foresman, J. B.; Ortiz, J. V.; Cui, Q.; Baboul, A. G.; Clifford, S.; Cioslowski, J.; Stefanov, B. B.; Liu, G.; Liashenko, A.; Piskorz, P.; Komaromi, I.; Martin, R. L.; Fox, D. J.; Keith, T.; Al-Laham, M. A.; Peng, C. Y.; Nanayakkara, A.; Challacombe, M.; Gill, P. M. W.; Johnson, B.; Chen, W.; Wong, M. W.; Gonzalez, C.; Pople, J. A. *Gaussian 03 (Revision C.02)*, Gaussian, Inc.: Wallingford CT, 2004.

(33) Becke, A. D. *Phys. Rev. A* **1988**, *38*, 3098.

(34) Lee, C.; Yang, W.; Parr, R. G. *Phys. Rev. B.* **1988**, *37*, 785.

(35) Becke, A. D. *J. Chem. Phys.* **1993**, *98*, 5648.

(36) Singh, U. C.; Kollman, P. A. *J. Comput. Chem.* **1984**, *5*, 129.

(37) Besler, B. H.; Merz, K. M.; Kollman, P. A. *J. Comput. Chem.* **1990**, *11*, 431.

(38) Cances, E.; Mennucci, B. *J. Math. Chem.* **1998**, *23*, 309.

(39) (a) Boys, S. F.; Bernardi, F. *Mol. Phys.* **1970**, *19*, 553. (b) Simon, S.; Duran, M.; Dannenberg, J. J. *J. Chem. Phys.* **1996**, *105*, 11024.

(40) Ponder, J. W. *TINKER: Software tool for molecular design*, 4.2 ed.; Washington University School of Medicine, 2004.

(41) Hoover, W. G. *Phys. Rev. A* **1985**, *31*, 1695.

(42) Allen, M. P.; Tildesley, D. J. *Computer Simulation of Liquids*; Clarendon Press: Oxford, U.K., 1989.

(43) Essmann, U. L.; Perera, M. L.; Berkowitz, T.; Darden, H.; Lee, H.; Pedersen, L. G. *J. Chem. Phys.* **1995**, *103*, 8577.

(44) Martínez, J. M.; Martínez, L. *J. Comput. Chem.* **2003**, *24*, 819.

(45) Jorgensen, W. L.; Maxwell, D. S.; Tirado-Rives, J. *J. Am. Chem. Soc.* **1996**, *118*, 11225.

(46) Ruckenstein, E.; Shulgin, I. *Fluid Phase Equilib.* **2001**, *180*, 281.

(47) Gmehling, J.; Li, J.; Schiller, M. *Ind. Eng. Chem. Res.* **1993**, *32*, 178.

(48) Alcalde, R.; Aparicio, S.; García, B.; Leal, J. M. *J. Phys. Chem. B* **2005**, *109*, 19908.

(49) Matteoli, E. *J. Phys. Chem. B.* **1997**, *101*, 9800.

(50) Müller, G.; Lutz, M.; Harder, S. *Acta Crystallogr.* **1996**, *B52*, 1014.
(51) McDermott, D. *J. Phys. Chem.* **1986**, *90*, 2569.
(52) Gómez-Gualdrón, D. A.; Aparicio, S.; Balbuena, P. B. *Ind. Eng. Chem. Res.* **2007**, *46*, 131.
(53) McDonald, D. D.; Dunay, D.; Hanlon, G.; Hyne, J. B. *Can. J. Chem. Eng.* **1971**, *49*, 420.
(54) (a) Vasilev, V. A.; Novikov, A. N. *Izv. Vyssh. Uchebn. Zaved. Khim. Khim. Tekhnol.* **1989**, *32*, 53. (b) Noll, O.; Fischer, K.; Gmehling, J. *J. Chem. Eng. Data* **1996**, *41*, 1434.
(55) García, B.; Aparicio, S.; Alcalde, R.; Dávila, M. J.; Leal, J. M. *Ind. Eng. Chem. Res.* **2004**, *43*, 3205.
(56) Zaichikov, A. M.; Russ, J. *Gen. Chem.* **2006**, *76*, 626.
(57) Aparicio, S.; García, B.; Alcalde, R.; Dávila, M. J.; Leal, J. M. *J. Phys. Chem. B* **2006**, *110*, 6933.
(58) (a) López, E. R.; García, J.; Fernández, J. *J. Chem. Eng. Data* **1999**, *44*, 309. (b) Horstmann, S.; Fischer, K.; Gmehling, J. *J. Chem. Eng. Data* **2004**, *49*, 1499.
(59) Marcus, Y. *Phys. Chem. Chem. Phys.* **1999**, *1*, 2975.
(60) Shulgin, I. L.; Ruckenstein, E. *J. Phys. Chem. B* **2006**, *110*, 12707.
(61) Shulgin, I. L.; Ruckenstein, E. *Phys. Chem. Chem. Phys.* **2008**, *10*, 1097.
(62) Guo, J. H.; Luo, Y.; Augustsson, A.; Kashtanov, S.; Runbensson, J. E.; Shuh, D. K.; Agren, H.; Nordgren, J. *Phys. Rev. Lett.* **2003**, *91*, 157401.
(63) Dixit, S.; Soper, A. K.; Finney, J. L.; Crain, J. *Europhys. Lett.* **2002**, *59*, 377.
(64) Aparicio, S.; Alcalde, R.; Leal, J. M.; García, B. *J. Phys. Chem. B* **2005**, *109*, 6375.
(65) Tumakaka, F.; Gross, J.; Sadowski, G. *Fluid Phase Equilib.* **2005**, *228*, 89.
(66) Barker, J. A.; Henderson, D. *J. Chem. Phys.* **1967**, *47*, 4714.
(67) Huang, S. H.; Radosz, M. *Ind. Eng. Chem. Res.* **1990**, *29*, 2284.
(68) Aparicio, S.; Hall, K. R. *Fluid Phase Equilib.* **2007**, *254*, 112.
(69) Wagner, W.; Pruss, A. *J. Phys. Chem. Ref. Data* **2002**, *31*, 387.
(70) Reuck, K. M.; Craven, R. J. B. Methanol: International Thermodynamic Tables of the Fluid State—12; Blackwell Science, 1993.

JP712131J